

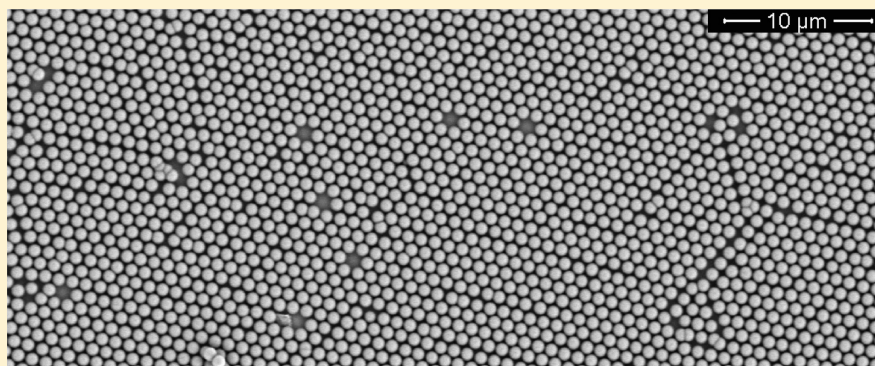
# Qualitative and Quantitative Analysis of Crystallographic Defects Present in 2D Colloidal Sphere Arrays

Víctor Canalejas-Tejero, Marta Ibisate, Dolores Golmayo, Alvaro Blanco,\* and Cefe López

Instituto de Ciencia de Materiales de Madrid ICMM-CSIC and Unidad Asociada CSIC-UVigo, C/Sor Juana Inés de la Cruz 3, 28049 Madrid, Spain

**S** Supporting Information

## ABSTRACT:



In this work, we present a study of the typical spontaneous defects present in self-assembled colloidal monolayers grown from polystyrene and silica microspheres. The quality of two-dimensional crystals from different colloidal suspensions of beads around 1  $\mu\text{m}$  in diameter has been studied qualitatively and quantitatively, evaluated in 2D hexagonal arrays at different scales through Fourier analysis of SEM images and optical characterization. The crystallographic defects are identified to better understand their origin and their effects on the crystal quality, as well as to find the best conditions colloidal suspensions must fulfill to achieve optimal quality samples.

## INTRODUCTION

Ordered monolayers (MLs) made of microspheres have interesting scientific and technological applications, mainly in the field of micro/nanofabrication,<sup>1,2</sup> where MLs can be used as useful patterns for soft lithography,<sup>3,4</sup> a versatile and cheap technique as compared with the most widespread photolithography. Another prominent application of these two-dimensional (2D) arrays of spheres lies in the field of photonics, and more recently, its application in plasmonics<sup>5</sup> has generated much interest. The quality of these ordered structures is subject to the crystalline defects. Note that we studied the defects only in ordered arrays due to the vast field of applications for these structures; further studies using different deposition methods for either ordered or disordered MLs could yield different values, which would increase the knowledge in this matter.

Natural assembly of colloidal submicrometer spheres is a simple and inexpensive approach for creating two and three-dimensional (2D and 3D) periodic structures.<sup>6,7</sup> In most cases, the building blocks are microspheres made of organic or inorganic material ordered in face-centered cubic crystal lattice structure. Both 2D and 3D photonic crystals (PCs) based on microspheres<sup>8,9</sup> can be prepared by vertical deposition method. Dimitrov et al.<sup>5</sup> and Palacios-Lidón et al.<sup>10</sup> studied the effect of

particle monodispersity, volume fraction, and environmental humidity on the size of the formed domains in MLs made by vertical deposition. Recently, Sun et al.<sup>11</sup> studied the self-assembly of colloidal spheres confined within wedge-shaped cells, and they prepared single-domain 2D colloidal crystals with centimeter size, the one used in the present work. Finally, the role of the meniscus shape has been studied in depth<sup>12</sup> at present.

The majority of the applications of ordered MLs of spheres require a precise and controlled incorporation of pre-engineered defects. Natural and pre-engineered defects have been extensively studied in previous works in 3D<sup>13–18</sup> and in 2D colloidal crystals<sup>19–21</sup> in order to understand their impact on the quality and their usefulness as intentional defects.

Crystallographic defects found in a ML made of microspheres can be classified in two different manners. Classic crystallographic classification of defects in any crystalline structure distinguishes between intrinsic defects, always present in any crystal and characteristic of the structure (vacancies, voids, poorly compacted or even empty areas, dislocations, rotated domains,

**Received:** August 12, 2011

**Revised:** November 7, 2011

**Published:** November 09, 2011

single spheres on top the ML and 3D arrangements), and extrinsic defects, which depend on the building blocks (impurities, deformed or different sized particles, or substrate imperfections). Here, building block quality is crucial for optimal growth, and one should start keeping polydispersity below 3% to minimize intrinsic defects. The second classification is made according to the defect dimension: point defects (0D: misshapen spheres, small interstitial particles, simple vacancies, vacancies caused by different size spheres or impurities, small impurities within the crystal structure), line defects (1D: grain boundaries, dislocations, double spheres, linear vacancies), planar defects (2D: multiple and nonlinear spheres linked by synthesis, rotated domains, substrate imperfections, nonlinear vacancies and multiple voids, poorly compacted zones), and bulk defects (3D: spheres mounted on the ML, clusters). All these factors cause disturbances and alterations in the lattice and therefore in the lattice parameter.

The aim of this work is to study the effect of spontaneous defects that limit the crystalline quality in PCs based on spherical microparticles grown by the wedge-shaped cell method.<sup>11</sup> Extrinsic defects derived from the lack of quality of the building blocks, as well as the intrinsic ones, have been analyzed in detail. Colloidal suspensions from different commercial suppliers, and also custom-made, have been used to prepare 2D arrays of micrometer spheres. MLs were prepared by the wedge method. Defects are characterized by scanning electron microscopy (SEM) and lattice order by Fourier transforms (FTs) of SEM images. ML quality has also been optically characterized.

## EXPERIMENTAL SECTION

Seven colloidal suspensions of polystyrene (PS) and silica (SiO<sub>2</sub>) spheres have been used. Six were acquired from different commercial suppliers; the remaining one was produced in our laboratory by Stöber synthesis. All the spheres are around 1  $\mu\text{m}$  in diameter due to the ease of finding this particle size from each manufacturer, and our results could be extrapolated to other sizes because of the sphere continuous growth synthesis process, although some differences could be found taking in account linked spheres. Note that they only show the quality of the specific batch we received and not the quality of the products of each manufacturer.

The chosen solvent was ultrapure H<sub>2</sub>O for both PS and SiO<sub>2</sub> spheres. During growth, commonly used ethanol or other alcohols were not used in this case for SiO<sub>2</sub> spheres because the evaporation rate was too fast, apart from the fact that water offered good results for both types of beads in the same growing conditions, except concentration. Suspension concentration was varied in the range 0.3–10% w/w for PS, and 0.3–2% for SiO<sub>2</sub>. All fabrication setup components (substrates and cover slides) in contact with the colloidal suspension were cleaned and hydrophilized using H<sub>2</sub>O<sub>2</sub> 30% at 80 °C for 45 min and 4 h for glass and Si substrates, respectively, then rinsed with distilled water and dried with N<sub>2</sub> flow. It is important to point out that, although substrate size is not a limitation for this fabrication method, in order to obtain a horizontal evaporation front and, therefore, a good sample, its size has to be larger than 10 mm wide.

MLs were prepared by the wedge-shaped cell method.<sup>11</sup> The angle between the bottom substrate where the ML grows and the top glass slide that completes the cell was always set at a fixed angle of  $\sim 2^\circ$  (Figure 1). This value provided us the best quality samples after several experimental tests. Double side polished silicon wafers (0.45 mm thick) were used as substrate, attached to the bottom glass. All samples were produced through an evaporation process inside a Binder KBF constant climate chamber, at controlled temperature and relative

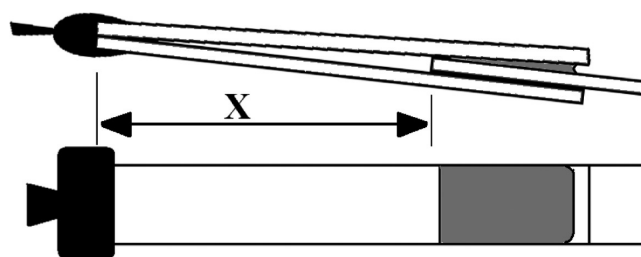


**Figure 1.** Scheme of the wedge-shaped cell system used in this work. Colloidal suspension is colored in gray. ML will grow on the middle (short) substrate. Best results were obtained for a tilt angle between  $5^\circ$  and  $30^\circ$  (upward meniscus evaporation) from the horizontal for the whole system. Optimized angle for 1  $\mu\text{m}$  spheres was about  $2^\circ$  between the two large glass substrates, fixed by measuring the distance X always the same.

humidity (from 20 to 50 °C and 90%, respectively). Deposition angle was optimized after scanning values between  $90^\circ$  and  $-90^\circ$ .

The SEM characterization protocol was carried out in the following way. A representative zone of each sample was mapped taking 25 SEM images at  $5000\times$ . Resultant images were merged and a  $5 \times 5$  mosaic was generated. Defects were classified and counted manually. Once all the defects were known, recorded, and listed, they were related to the lattice order by analyzing their FTs at different scales. In addition, MLs transmittance ( $T$ ) was measured using a Fourier transform spectrometer Bruker IFS 66/S attached to a microscope with a  $4\times$  objective at normal incidence.

## RESULTS AND DISCUSSION

Table 1 shows the characteristics of the colloidal suspensions of polystyrene (PS) and silica spheres and their suppliers. Diameters (in micrometers), size distribution claimed by the manufacturer, and those measured in this work are also shown, as well as the estimated number of spheres of the total measured zone by SEM. The coefficient of variation (CV) is the size distribution (standard deviation) as a percentage of the diameter.

Volume concentration of the suspension is a critical factor. Optimal concentrations were 0.5% w/w and 1.25% w/w for PS and SiO<sub>2</sub>, respectively. Optimal growth conditions were established after a systematic study varying temperature and relative humidity. Obtained values imply very slow evaporation rates (20 to 25 °C, 90% RH), with evaporation times usually shorter than 24 h for volumes from 40  $\mu\text{L}$  to 100  $\mu\text{L}$ . The optimized angle of the whole system resulted in values between  $5^\circ$  and  $30^\circ$  tilt, taking into account upward meniscus evaporation (between  $-5^\circ$  and  $-30^\circ$  from the horizontal). Figure 2 shows different types of defects and an ordered zone obtained on samples grown under optimized growth conditions. All of the defects can be seen in the Supporting Information.

In order to check the effect of extreme concentrations, we have prepared very low and very high concentrated suspensions, finding quite different arrangements from those prepared at optimal conditions. Samples grown using very low concentration ( $<0.3\%$  w/w) have an appearance resembling a Sierpinski triangle fractal structure. This behavior has also been observed in the last stage of a ML growth process, when the concentration decreases sharply, disrupting the growth of a compact ML. Under these unusual growth conditions, a  $60^\circ$  rotation of the crystal lattice relative to the compact ML properly grown (Figure 3a) is obtained, having the same growth pattern found in 2D–3D

**Table 1. Specifications of the Colloidal Suspensions and Total Quantity of Beads in the Studied Zone<sup>a</sup>**

colloidal suspension	A	B	C	D	E	F	G
material and characteristics	PS	PS	PS	PS (surface sulfate modified)	PS	SiO <sub>2</sub>	SiO <sub>2</sub>
Size and Quality Claimed by the Manufacturer							
sphere diameter ( $\mu\text{m}$ )	1	0.978	1.025	0.99	0.984	-	1.160
size distribution C.V. (%)	$\leq 3$	3.27	0.98	1.4	$\leq 6$	-	4.31
Size and Quality Measured in This Work (SEM analysis)							
sphere diameter ( $\mu\text{m}$ )	1.03	0.96	1.04	1.01	0.98	0.92	1.23
size distribution C.V. (%)	2.96	1.25	6.63	0.86	2.91	1.26	4.10
Estimated Number of Spheres of the Total Measured Zone by SEM for Defect Analysis							
number of spheres	70125	84388	20736 <sup>b</sup>	73185	106602	56848	47897

<sup>a</sup> Sample classification is related to different brands. The list of manufacturers is as follows: (A) Duke Scientific, (B) Microparticles GmbH, (C) Polybead-Polysciences, (D) Invitrogen, (E) Ikerlat, (F) custom-made by Stöber synthesis in our laboratory, (G) Microparticles GmbH. <sup>b</sup> The measurable area for sample C was not big enough to acquire similar number of images.

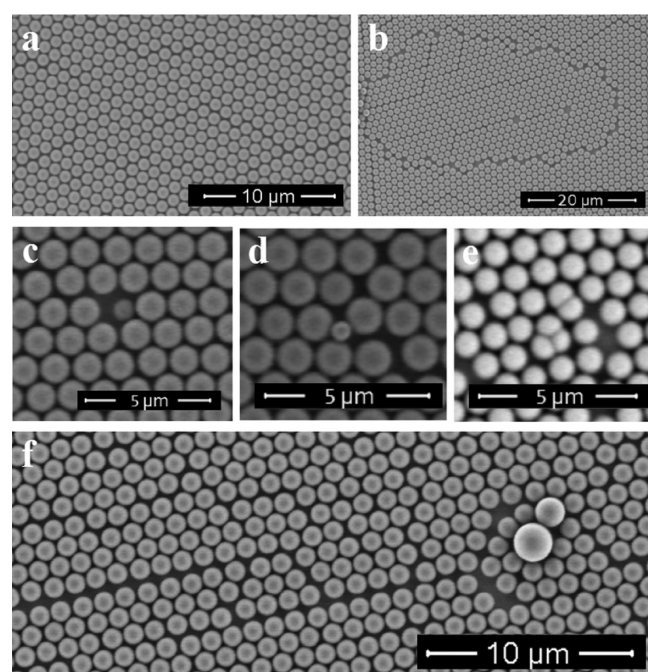


**Figure 2.** (a) Ordered zone, (b) rotated domain with a pair of vacancies, (c) vacancy with smaller sphere, (d) interstitial smaller sphere, (e) SiO<sub>2</sub> linked spheres, (f) bigger spheres causing lattice distortion and dislocations.

crystals obtained by vertical deposition. Then, MLs properly grown by the wedge system always show the left pattern indicated in Figure 3a, except in the typical sharp and very small zones obtained when the colloidal suspension is near to losing its capacity of growing more 2D compact layers. These differences in geometric orientation could be induced by the concentration of the colloidal suspension or the position of the substrate (near-horizontal for 2D MLs grown by the wedge system, and near-vertical for vertical deposition system). Further studies in this matter would be interesting to shed light on the growing mechanism. In the other extreme, 2D–3D dendritic structures (Figure 3b) were generated using higher concentrations (10% w/w) while keeping the rest of our optimal growth conditions previously mentioned. These dendritic formations grew on the bottom side of the top glass slide in the wedge-shaped cell system

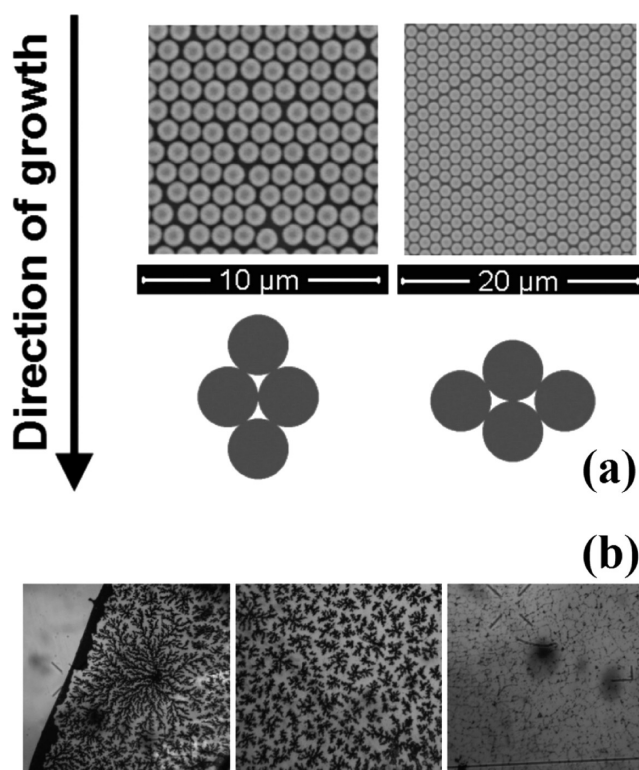


**Figure 3.** (a) SEM images showing the growth scheme of monolayers grown in optimal conditions (left) and using low concentration (right). 60° angle is the difference between them. The picture at the right represents the same growth pattern found in 2D–3D crystals obtained by the vertical deposition method. (b) Some of the dendritic formations obtained at concentrations around 10% w/w. Images were taken with microscope at 4 $\times$  and the side of each picture is 0.5 mm.

we used, presenting order at a very short range and disorder at medium and long range.

Figure 4 shows representative SEM images of each batch. A large number and variety of defects in samples of poorer quality are observed. Better quality MLs (A, B, D, and G) stand out easily because of the high level of order and array homogeneity. We observed that even the best samples we produced always had crystallographic defects in the form of vacancies.

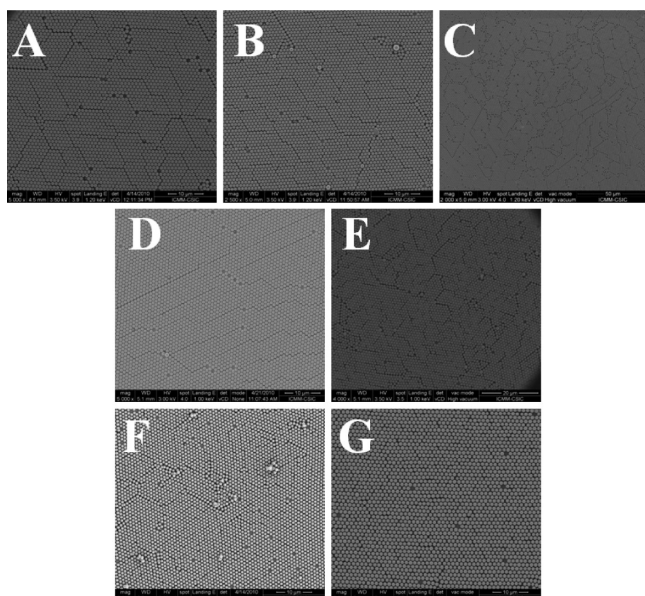


**Figure 4.** SEM images of each ML grown in optimal conditions. The area of every individual image is about  $2800 \mu\text{m}^2$ .

**Table 2. Extrinsic Defects<sup>a</sup>**

monolayer/ extrinsic defects	A	B	C	D	E	F	G
0D							
Small spheres	8.47	2.24	39.59	1.41	1.92	1.71	3.86
Big spheres	0.10	2.06	0	0.74	1.84	0	0
Impurities	0.33	0.17	0.05	0.01	0.47	0.62	0.36
0D/1D							
Impurities on the lattice	0.43	0.07	0	0	0.10	0.07	0.23
2D							
Substrate imperfections <sup>b</sup>	1	0	1	2	0	0	1
2D/3D							
Linked and deformed spheres	0.11	1.72	0.10	0	9.11	26.58	2.80

<sup>a</sup> Results are expressed in % of the total estimated number of spheres of the merged image from 25 SEM pictures. <sup>b</sup> Real quantity of these kinds of defects found in the MLs.

**SEM Images Analysis.** Using optimized conditions, ML samples of several square centimeters and good quality can be grown. Table 2 shows the type and number of extrinsic defects found after SEM analysis of the samples prepared from the seven different colloidal suspensions (from A to G). Results are expressed in % of the total estimated number of spheres except for the very rare defects (marked with <sup>b</sup>); for better understanding, their number is the real quantity of these kinds of defects found in the MLs (note that the number of very rare defects is related to different total values of spheres, indicated in Table 1). These extrinsic defects are mainly different-sized beads and linked particles (bimodal particles). Impurities are usually very small particles with no defined shape made of the same or different material that comes within the colloidal suspensions. Once the ML is grown, impurities normally occupy interstitial positions and rarely are they over the ML (called “Impurities on

**Table 3. Intrinsic Defects<sup>a</sup>**

monolayer/ intrinsic defects	A	B	C	D	E	F	G
0D							
vacancies	3.19	1.75	0.88	2.70	1.61	3.16	1.52
vacancies due to big or deformed spheres	0	0.40	0	0	0.82	0	0
vacancies with/due small sphere	3.34	2.13	7.33	1.31	0.40	1.37	3.55
1D							
dislocations	0.91	0.39	1.93	0.44	0.57	1.64	1.13
1D/2D							
multiple voids	0.09	0.10	0.05	0.03	0.13	0.04	0.13
multiple voids with/due small spheres	0.13	0	0.53	0	0	0	0
multiple voids with/due big or deformed spheres	0	0.21	0	0	0.24	0	0
poorly compacted areas	0.20	0.69	1.88	0.10	0.72	1.39	0.84
domains <sup>b</sup>	1	2	13	3	20	9	4
3D							
single sphere on the monolayer <sup>b</sup>	1	0	0	2	1	31	0
clusters and 3d stacks <sup>b</sup>	0	1	0	3	2	75	0

<sup>a</sup> Results are expressed in % of the total estimated number of spheres of the merged image from 25 SEM pictures. <sup>b</sup> Real quantity of these kind of defects found in the MLs.

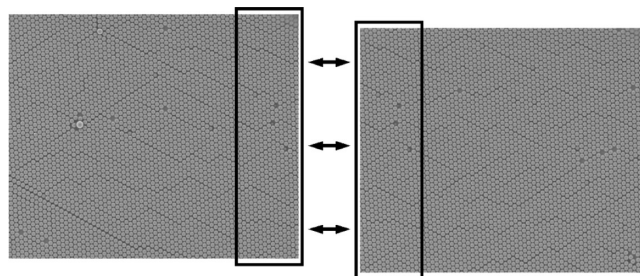


**Figure 5.** Coincident regions of two individual and consecutive SEM images are shown for illustrate the merging process.

the lattice” in Table 2). We considered impurities on the lattice as 0D defects or 1D defects taking in account the shape of their disruptive effect on the spheres array. Substrate imperfections are slight grazes or scratches and they can produce highly disruptive effects, depending on their size. Substrate imperfections we found were extremely small and short grazes with no important effects on the number of other defects. Spheres were considered large or small when they exceeded the average diameter by 10%. On PS spheres, A and C colloidal suspensions had a high percentage of small particles, but C has by far the highest number of small microspheres, with a huge quantity of microspheres of diameter lower than  $0.5 \mu\text{m}$ . Sample B has many particles whose shape was cylindrical rather than spherical; B and E had the highest number of big particles, those in B generally with a diameter from 1.5 to 2 times the average diameter; E has two very different types of spheres attending to their surface roughness

(typical finish and highly eroded finish). Besides, deformed and bonded spheres were present in a high quantity in E. Regarding the SiO<sub>2</sub> samples, diameter of the spheres of sample G fluctuates significantly between 1132 and 1312 nm; deformed and bonded spheres were present in high quantity in F and G samples.

Intrinsic defects are shown in Table 3. A domain was considered rotated when the rotation angle was  $\geq 5^\circ$ . Not all the intrinsic defects show a clear relation with extrinsic defects, but in the case of rotated domains, this relation appears more clearly: sample C, with a great amount of small spheres, owns a high number of dislocations, poorly compacted zones, and rotated domains. Sample E, with two different types of spheres attending to their surface finish, has an important number of rotated domains. The high number of distorted and multiple particles in F produces multidomain MLs and a large quantity and variety of 1D and 2D intrinsic defects. Indeed, the big amount of dislocations in samples C and F seems to be related to the large quantity of particles of different size or shape. Other intrinsic defects, like vacancies or voids, are more difficult to relate to the existence of particles of different size, and their disruptive effect seems to be absorbed by the structure at very short range.

**Fourier Transform Analysis.** Lattice order was analyzed from FTs of SEM images at two different scales for each sample: from an individual SEM image (around  $55 \times 50$  spheres) and including the full mapping of 25 SEM pictures. Full mapping was done by a digital photomerge process using coincident regions of consecutive SEM images (Figure 5). In all cases, SEM merged images were combined after data box removal of the pictures. Figure 6 shows FTs for all the samples.

There is a clear connection between disorder and the number of different crystalline domains (Table 3), shown as multiple or diffused dots in the FT pattern. FTs identify the best quality samples (A, B, D, and G) regardless of the measured area. Samples A and B had the lowest number of crystalline domains (1 and 2, respectively) and exhibited less image size dependence of FT pattern. Sample D shows three rotated domains that cause the sharp distortion in the FT image of the full area. G has a larger amount of domains, and the FT pattern shows 4 rotated domains. Samples C, E, and F, with a high number of domains, are more disordered, increasing with greater area under consideration, and showing ring-like patterns accordingly. Besides, note that different domain orientations do not deteriorate optical qualities; only domain boundaries do.

**Optical Measurements and Multidomains.** Sample quality was also analyzed by measuring  $T$  in the IR region, which is a way to estimate the diffusing power for a given thickness (in this case, 1 ML, around  $1 \mu\text{m}$ ). These measurements were done for two different sample areas ( $300$  and  $800 \mu\text{m}$ ) defined by employing two different optical microscope apertures in order to compare short- and long-range order. Figure 7 shows  $T$  spectra plotted versus  $\omega$  (energy dimensionless units,  $\omega = \sqrt{3} d_{\text{sph}}/(2\lambda)$ ,  $d_{\text{sph}}$  is the sphere diameter and  $\lambda$  is the wavelength of light) for all the samples.

Observed dips in  $T$  spectra are a consequence of light coupling to guided modes inside the ML and their quality factor ( $Q$ ) is related with sample quality.  $Q$  was calculated by dividing  $\lambda$  by  $\Delta(\lambda)$  for the lower energy dip (same position as the peak labeled with an arrow in Figure 7, graph A). The results, plotted in Figure 8, are consistent with those obtained from the FT's. Samples B and D had the best  $Q$ . This result indicates that B and D as the best colloidal suspensions, regardless of the significant number of nonspherical particles (cylindrical shape) and large

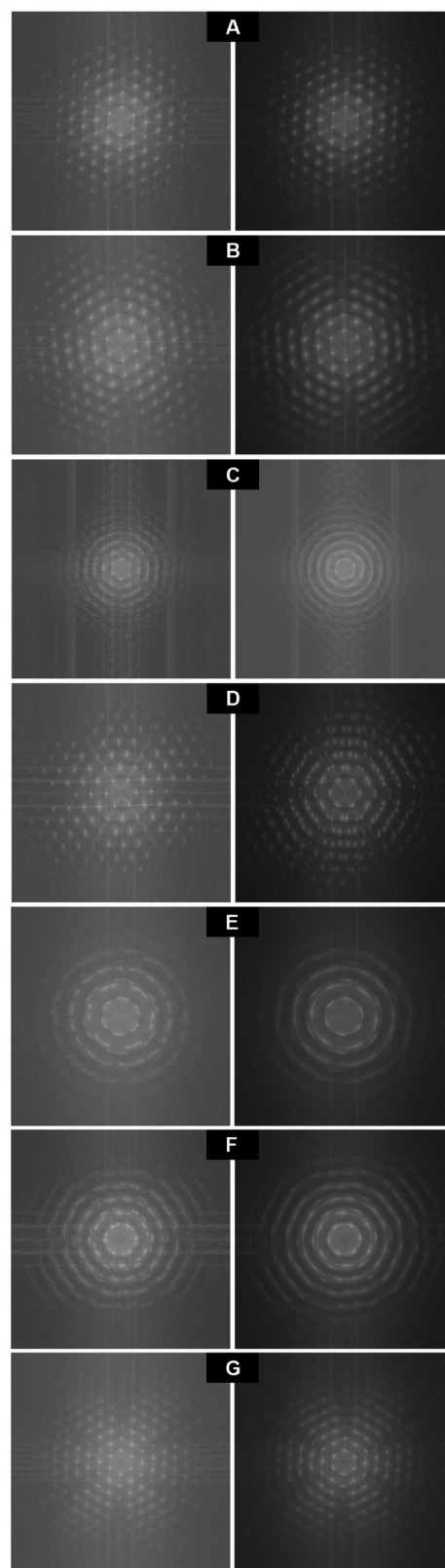


**Figure 6.** FTs of SEM images. In each sample, left picture is from an individual SEM image (around  $55 \times 50$  spheres), and right picture includes the full mapping (25 individual images). Diffuse ring-like patterns indicate the presence of multidomains.

spheres ( $1.5\text{--}2 \mu\text{m}$ ) in sample B, followed by A, G, and E. When  $T$  is measured, different behavior is observed when different

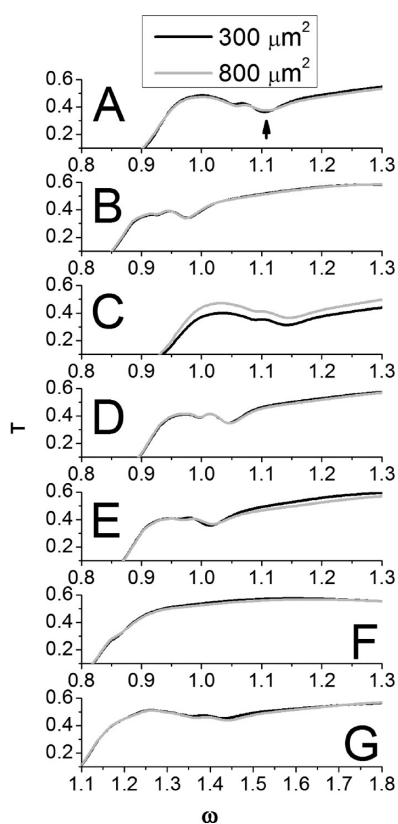


**Figure 7.** Plot of  $T$  versus  $\omega$  for all the MLs. Arrow in the graph of sample A indicates the low energy peak used for  $Q$  calculation. (Note that graph G has different  $\omega$  scale due to a significantly larger size).

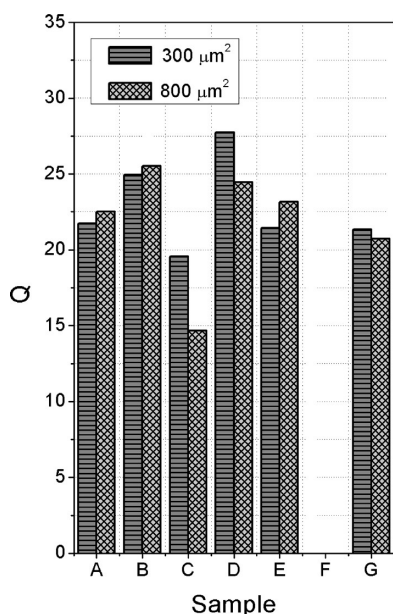


**Figure 8.**  $Q$  values obtained after optical characterization. Highest quality colloidal suspensions presented higher  $Q$  values. Sample F did not present a defined peak due to the extremely low quality of the lattice.

aperture is employed. Thus, an improvement in the quality for larger iris aperture, revealing better quality for larger areas, is present in samples A, B, and E, and a huge decrease in the quality

is detected in samples C and D, probably because the number of defects (mainly different crystalline domains) in the measurement of the smaller area ( $300 \mu\text{m}^2$ ) was significantly lower than average.

Apart from the previous result, a slight  $Q$  variation in samples A, B, and G might be taken as a significant result in order to choose a good colloidal suspension attending to tiny changes in quality at different scales.

We have found experimentally that the size distribution offered by commercial companies can be reflected in very different ways attending to sphere size and shape. Thus, monodispersity is the key for high quality, as expected. But not all the intrinsic defects have similar effects. So, we found two main limiting factors for obtaining perfect 2D hexagonal arrays of microspheres made by the wedge system: first, the lack of size uniformity, especially if there are great numbers of small spheres with diameter around 0.5 to 0.9 times the average diameter—much smaller particles have low influence on the quality of the final structure because they tend to occupy interstitial positions; second, the great amount of deformed, malformed, or bonded spheres produced during the synthesis—these kinds of extrinsic defects are the cause of intrinsic defects such as dislocations and rotated domains, where the last produce the main effect regarding crystal disorder. Other intrinsic defects such as vacancies, voids, and poorly compacted zones will always be present in nonpatterned substrates, as occurs in crystals grown in nature (although their impact on the quality of the ML is lower), because perfect crystals are only ideal models of ordered spatial points occupied by atoms or molecules, but in the real world, crystal growth dynamics produce a large variety of crystallographic defects.

## CONCLUSIONS

Different colloidal suspensions of PS and  $\text{SiO}_2$  spheres of approximately  $1 \mu\text{m}$  in diameter have been studied in our comparative experiment in order to identify the factors that determine the quality of 2D hexagonal arrays built using the wedge system, being a method that imitates natural crystal growing and all the inherent crystallographic defects associated with it.

For this purpose, crystallographic defects have been analyzed qualitatively and quantitatively. ML disorder has been analyzed by counting defects using SEM images and FT's of SEM pictures, and related to optical quality. So, seven ordered MLs from different manufacturers were studied and compared to each other.

We have found two main limiting factors for obtaining single domain 2D hexagonal arrays. The first one is the lack of size uniformity, especially if there are great amounts of spheres smaller than the average diameter in samples with low quantity of linked and/or deformed spheres, as seen in SEM and FT image analysis from sample C, confirmed with its high number of crystalline domains, a consequence of such a high number of small spheres, and with optical measurements. The second one is the presence of nonspherical particles and/or linked spheres produced during the synthesis, like in samples E and F, resulting in a high number of rotated domains, as seen in SEM and FT images, giving rise to disorder, confirmed with optical measurements. Then, both types of extrinsic defects are the cause of intrinsic defects such as dislocations and rotated domains, the last producing the main effect regarding crystal disorder at medium and long range. Thus, the constraints offered by the growth

method we used are reflected in short-range order and long-range disorder due to the presence of different sized and/or shaped particles.

On the other hand, we detected the best quality MLs through SEM and FT images (A, B, D, and G samples), confirmed with transmission measurements, which selected the top-quality MLs (B and D). Most important characteristics in common were very low size distribution, low quantities of different sized particles, virtual absence of impurities, and very low proportion of deformed or linked spheres.

Finally, we can consider quality in two different ways depending on the size of the ML we need for our purposes: taking into account the higher  $Q$  value, or weighing the smaller variation in quality up at different scales.

## ■ ASSOCIATED CONTENT

**S Supporting Information.** SEM images of all kind of crystallographic defects we found in our samples. Sphere diameter is about 1  $\mu\text{m}$  in all cases. This material is available free of charge via the Internet at <http://pubs.acs.org>.

## ■ ACKNOWLEDGMENT

This work was partially supported by EU FP7 NoE Nanophotonics4Energy grant no. 248855; the Spanish MICINN CSD2007-0046 (Nanolight.es), MAT2009-07841 (GLUSFA), CSIC PIF08-016 and Comunidad de Madrid S2009/MAT-1756 (PHAMA) projects.

## ■ REFERENCES

- (1) Li, Y.; Koshizaki, N.; Cai, W. *Coord. Chem. Rev.* **2011**, *255*, 357–373.
- (2) Li, Y.; Cai, W.; Duan, G. *Chem. Mater.* **2008**, *20* (3), 615–624.
- (3) Xia, Y.; Whitesides, G. M. *Angew. Chem., Int. Ed.* **1998**, *37*, 550–575.
- (4) Rogers, J. A.; Nuzzo, R. G. *Mater. Today.* **2005**, *8*, 50–56.
- (5) López-García, M.; Galisteo-López, J. F.; Blanco, A.; Sánchez-Marcos, J.; López, C.; García-Martín, A. *Small* **2010**, *16* (6), 1757–1761.
- (6) Zhang, J.; Li, Y.; Zhang, X.; Yang, B. *Adv. Mater.* **2010**, *22*, 4249–4269.
- (7) Galisteo-López, J. F.; Ibisate, M.; Sapienza, R.; Froufe-Pérez, L. S.; Blanco, A.; López, C. *Adv. Mater.* **2011**, *23*, 30–69.
- (8) Dimitrov, A. S.; Nagayama, K. *Langmuir* **1996**, *12*, 1303–1311.
- (9) Jiang, P.; Bertone, J. F.; Hwang, K. S.; Colvin, V. L. *Chem. Mater.* **1999**, *11*, 2132–2140.
- (10) Palacios-Lidón, E.; Juárez, B. H.; Castillo-Martínez, E.; López, C. *J. Appl. Phys.* **2005**, *97*, 063502.
- (11) Sun, J.; Tang, C. J.; Zhan, P.; Han, Z.; Cao, Z. S.; Wang, Z. L. *Langmuir* **2010**, *26* (11), 7859–7864.
- (12) Born, P.; Blum, S.; Munoz, A.; Kraus, T. *Langmuir* **2011**, *27*, 8621–8633.
- (13) Braun, P. V.; Rinne, S. A.; García-Santamaría, F. *Adv. Mater.* **2006**, *118*, 2665–2678.
- (14) A. Rinne, S.; García-Santamaría, F.; Braun, P. V. *Nat. Phot.* **2008**, *2*, 2662–2664.
- (15) Vlasov, Y. A.; Astratov, V. N.; Baryshev, A. V.; et al. *Phys. Rev. E* **2000**, *61*, 5784–5793.
- (16) Qi, M. H.; Lidorikis, E.; Rakich, P. T.; et al. *Nature* **2004**, *429*, 538–542.
- (17) Tetreault, N.; Mihi, A.; Miguez, H.; et al. *Adv. Mater.* **2004**, *16*, 346.
- (18) Palacios-Lidón, E.; Galisteo-López, J. F.; Juárez, B. H.; López, C. *Adv. Mater.* **2004**, *16* (4), 341–345.

- (19) Lechner, W.; Dellago, C. *Soft Matter* **2009**, *5*, 2752–2758.
- (20) E. Skinner, T. O.; A. L. Aarts, D. G.; A. Dullens, R. P. *Phys. Rev. Lett.* **2010**, *105*, 168301.
- (21) Gerbode, S. J.; Ong, D. C.; Liddell, C. M.; Cohen, I. *Phys. Rev. E* **2010**, *82*, 041404.